The Journal of Experimental Biology 204, 2251–2263 (2001)
Printed in Great Britain © The Company of Biologists Limited 2001
JEB 3484

LOCOMOTION IN SCOMBRID FISHES: VISUALIZATION OF FLOW AROUND THE CAUDAL PEDUNCLE AND FINLETS OF THE CHUB MACKEREL *SCOMBER JAPONICUS*

JENNIFER C. NAUEN* AND GEORGE V. LAUDER

Department of Organismic and Evolutionary Biology, Harvard University, Cambridge, MA 02138, USA

*e-mail: jnauen@oeb.harvard.edu

Accepted 18 April 2001

Summary

Scombrid fishes are known for high-performance locomotion; however, few data are available on scombrid locomotor hydrodynamics. In this paper, we present flow visualization data on patterns of water movement over the caudal peduncle and finlets (small fins on the dorsal and ventral body margin anterior to the caudal fin). Chub mackerel, *Scomber japonicus*, ranging in fork length from 20 to 26 cm, swam steadily at 1.2 fork lengths s^{-1} in a recirculating flow tank. Small, reflective particles in the flow tank were illuminated by a vertical (*xy*) or horizontal (*xz*) laser light sheet. Patterns of flow in the region near the caudal peduncle were measured using digital particle image velocimetry. Patterns of flow along the peduncle and finlets were quantified using manual particle tracking; more than 800 particles were tracked for at least 12 ms over a series of tailbeats from each of four fish.

In the vertical plane, flow trajectory and flow speed were independent of the position of the finlets, indicating that the finlets did not redirect flow or affect flow speed. Along, above and below the trailing surface of the peduncle, where the finlets were oriented along the peduncular surface, flow was convergent. Along, above and below the leading surface of the peduncle, where the finlets were absent, the flow trajectory was effectively horizontal. The lack of divergent flow on the leading surface of the peduncle is consistent with cross-peduncular flow formed by the lateral motion of the peduncle interacting with convergent flow resulting from forward movement of the body.

In the horizontal plane, particles illuminated by the *xz* light sheet situated approximately 3 mm below the ventral body surface were tracked within the laser light sheet for up to 40 ms, indicating strong planar flow. As the peduncle decelerates, the most posterior finlet is frequently at an angle of attack of at least 20 ° to the incident flow, but this orientation does not result in thrust production from lift generation. Finlet 5 does redirect cross-peduncular flow and probably generates small vortices undetectable in this study. These data are the first direct demonstration that the finlets have a hydrodynamic effect on local flow during steady swimming.

Key words: locomotion, swimming, scombrid fish, flow, finlet, particle tracking, mackerel, *Scomber japonicus*.

Introduction

Fish in the family Scombridae show a characteristic morphology of reduced body mass (narrow-necking) at the caudal peduncle, the presence of small non-retractable fins or ‘finlets’ spanning the dorsal and ventral margins of the body between the second dorsal and anal fins and the caudal fin (anterior to and along the peduncle) and the presence of raised bony structures or caudal keels on the lateral surface of the caudal fin (Collette and Nauen, 1983). The caudal peduncle and fin function as a force transmission mechanism and propeller for the most derived members of the group, the tunas (Knower and Shadwick, 1999).

The ubiquitous presence of finlets on the high-performance scombrid fishes and the proximity of these structures to the caudal fin have led to hypotheses that the finlets are accessory locomotory structures. Walters (Walters, 1962) proposed that finlets prevent roll and direct flow longitudinally along the body into the region between the caudal keels, where flow is then accelerated. Webb (Webb, 1975) and Lindsey (Lindsey, 1978) postulated that finlets deflect water across the caudal peduncle and enhance locomotory performance by preventing separation of the boundary layer and thus reducing drag. Magnuson (Magnuson, 1970) proposed that finlets direct water across the pronounced central caudal keel of tuna, thereby contributing to any lift forces produced at the keel.

As a first approach to testing these hypotheses, we previously quantified finlet kinematics during gliding and steady swimming of a more basal scombrid, the chub mackerel *Scomber japonicus* (Nauen and Lauder, 2000; Nauen and Lauder, 2001). *S. japonicus* has a dorsal set and a ventral set of five finlets, numbered here from 1 (rostral) to

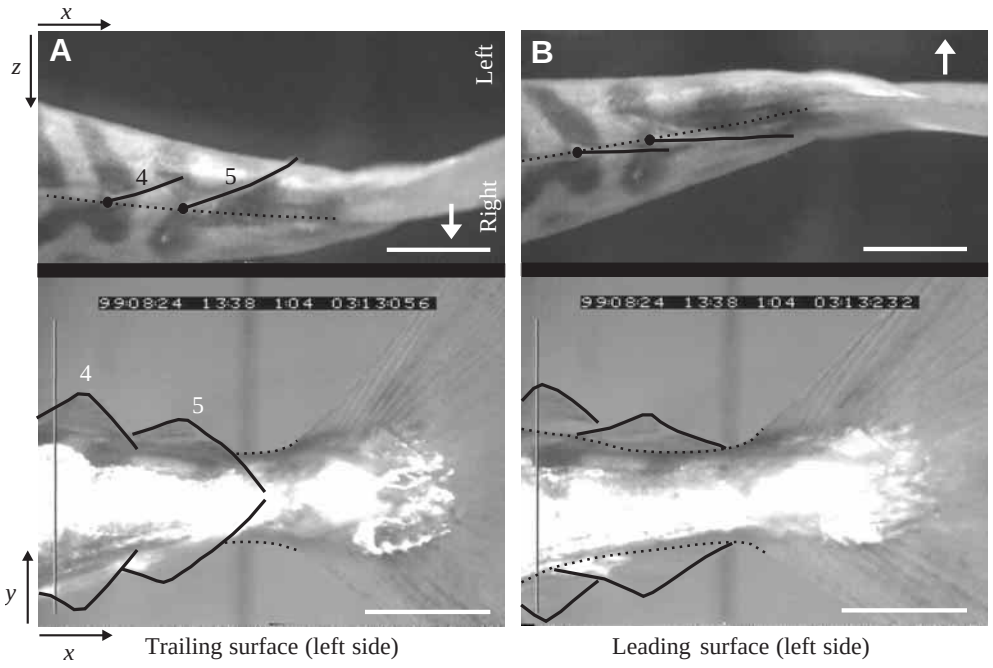

Fig. 1. Dorsal (*x*, *z* axes, viewed using a mirror, upper panels) and lateral (*y*, *x* axes, lower panels) views of the trailing (A) and leading (B) surfaces of finlets 4 and 5 and the caudal peduncle of a mackerel 22 cm in fork length (*FL*) during the deceleratory phase of a stroke at a steady swimming speed of 1.2 *FL* s^{-1}. The dorsal and lateral views are synchronous; time is shown in the lower field only. The outer finlet margin is outlined with the filled line; the circle indicates the anterior attachment point of each finlet. The finlets oscillate from the left (A) to the right (B) side of the dorsal and ventral body midlines (dotted lines) during the stroke and reach maximum excursions (note the tips of dorsal and ventral finlets 5 touching at the lateral midline of the body in the lower panel of A) on the trailing surface of the peduncle as the peduncle decelerates (the case shown in A is the left surface of the peduncle as it decelerates to the right). Scale bars (white lines) represent 1 cm; white arrows show the direction of tail movement.

5 (caudal). During steady swimming, the finlets typically oscillate symmetrically around the dorsal and ventral body midline in the horizontal plane. Maximum horizontal and vertical excursions of the finlets occur as the peduncle decelerates at the end of each stroke (Nauen and Lauder, 2000). An example of these movements is depicted in Fig. 1A, in which the finlets are in view along the trailing surface of the peduncle (the left surface of the peduncle as it decelerates to the right; lateral view Fig. 1A). The large size of finlet 5 and the narrow-necking of the caudal peduncle result in the tips of the dorsal and ventral fifth finlets meeting at the lateral midline of the trailing peduncular surface (Fig. 1A). As the peduncle decelerates in the opposite direction, the finlets are out of view along the leading surface (Fig. 1B).

Angle of attack (α) calculations, based on two-dimensional kinematic measurements and the assumption that the path of motion of the finlets approximates the direction of flow local to the finlet, indicated that during steady swimming finlet α values averaged approximately 0° over a tailbeat. Thus, we concluded that the finlets were not contributing to thrust production *via* classical lift-based mechanisms (Nauen and Lauder, 2000). We noted, however, that because the peduncle and caudal fin decelerated during the last half of each stroke (Fig. 1A) the finlets were positioned to direct some flow longitudinally into the developing caudal fin vortex (fig. 12 in Nauen and Lauder, 2000). On the basis of the position of the finlets during deceleration, we proposed that finlets alter flow trajectory and direct flow into the caudal fin vortex, thus increasing thrust production.

In this paper, we test this hypothesis and provide the first general picture of flow around the caudal peduncle of a scombrid fish. We used digital particle image velocimetry and particle-tracking techniques to determine the speed and trajectory of flow in the vicinity of the finlets and caudal peduncle of the chub mackerel *Scomber japonicus*. We quantified flow in both the vertical (*xy*) and horizontal (*xz*) planes. As a test of the vortex enhancement hypothesis, we compared the speed and trajectory of particles in the region of the finlets and peduncle as well as above and below these structures on the leading and trailing surfaces of the peduncle during the deceleratory phase of the tail stroke. We predicted that particle speed would be independent of finlet position, but that particle trajectory would be dependent on the position of the particles relative to the finlets and caudal peduncle, with the large movement of finlets across the trailing surface of the peduncle as the caudal fin decelerates at the end of each stroke (Fig. 1A) creating convergent flow along the body. To test the validity of our previous angle of attack measurements calculated from kinematic data, we also quantified the trajectory of flow in the horizontal plane relative to the orientation of the most posterior ventral finlet.

Materials and methods

Animals

Chub mackerel, *Scomber japonicus* (Houttuyn), were collected by fishing from various locations in coastal southern California, USA. The mackerel were fed chopped fish and housed in 1200 l tanks at a water temperature of 18±2 °C in a 12 h:12 h light:dark photoperiod.

Flow visualization

Experiments were conducted using a 600 l recirculating flow tank. The flow tank has a working area 82 cm long × 28 cm wide × 28 cm high. Water temperature was 19±1 °C. Flow speed in the tank was controlled using a variable-speed motor (details of the flow tank and calibration of flow speed have been presented previously; see, for example, Jayne et al., 1996; Gibb et al., 1999). We used a flow tank, rather than have the mackerel swim across the field of view of the cameras in still water conditions, to view the small (of the order of 1 cm) individual finlets for a series of sequential tailbeats at a specific speed of 1.2 fork lengths s^{-1} (*FL* s^{-1}).

As in previous studies (Drucker and Lauder, 1999; Wilga and Lauder, 1999; Drucker and Lauder, 2000; Lauder, 2000; Wilga and Lauder, 2000), flow was visualized by seeding the water with near-neutrally buoyant 12 µm diameter silver-coated glass beads (density 1.3 g cm^{-3}, Potters Industries, USA) that reflected light from a 5 W argon-ion laser. Images of the reflected light were recorded with a two-camera NAC high-speed video system at 250 fields s^{-1}. Images in Fig. 2 and Fig. 5 provide examples of the density of particles in the flow.

The laser light sheet was oriented in either the vertical (*xy*) or horizontal (*xz*) planes. The vertical light sheet was approximately 2 mm thick and 10 cm wide and was positioned in the center of the working section of the flow tank. The peduncle of the mackerel beat through the vertical light sheet (Fig. 2) as the fish swam. Images of the peduncle were recorded using one camera. The point in the stroke when the peduncle intersected the sheet (e.g. midstroke or during deceleration) varied when the mackerel moved slightly to its left or right. This allowed us to record flow around the finlets and caudal peduncle at different points in the stroke during separate tailbeats. The field of view of the camera was approximately 6 cm×4 cm and was scaled by recording images of a ruler at the beginning of each experiment. The relatively small field of view, necessary to image finlets that are of the order of 1 cm in length, restricted the view of the fish to the posterior 20 % (approximately). Note that the vertical light sheet was projected from below the tank, so that as the tail beat through the light sheet the body blocked the sheet, and flow immediately above that area was not illuminated (e.g. the dark areas in the top left side of Fig. 2A,B). Images of four animals ranging in fork length (*FL*) from 20 to 24 cm swimming at 1.2 *FL* s^{-1} were recorded.

The horizontal light sheet was approximately 2 mm thick and 10 cm wide and was positioned in the middle of the water column. When mackerel swam in the middle of the tank, the finlets intersected the light sheet, and images of flow in the region of the finlets were recorded. A ventral view of the mackerel and light sheet was recorded with a camera that viewed a front-surface mirror set at 45 ° beneath the tank. A second camera viewed the surface of the tank for a lateral view of the left side of the mackerel. The fields of view of the cameras were approximately 6 cm×4 cm and were scaled at the beginning of each experiment by recording an image of a ruler. Images were recorded of four animals (three of which were also used for the vertical light sheet experiments) ranging in length from 22 to 26 cm swimming at 1.2 *FL* s^{-1}.

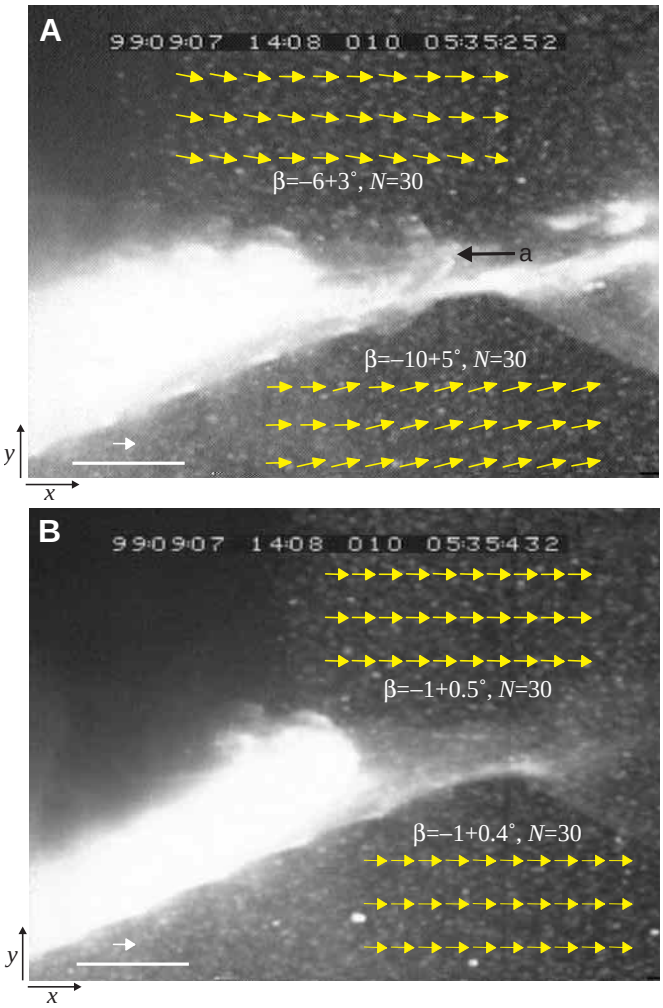

Fig. 2. Lateral view of the trailing surface of the caudal peduncle [A, note that the tips of the dorsal and ventral fifth finlets meet at the lateral body midline (a) on the trailing surface of the caudal peduncle] and the leading surface of the peduncle (B, note that the finlets are not visible along the peduncle) of a 24 cm fork length (*FL*) mackerel during the deceleration phase of the stroke at a steady swimming speed of 1.2 *FL* s^{-1}. The flow is seeded with reflective glass beads and illuminated by a vertically oriented laser light sheet. Velocity vectors in yellow were calculated using digital particle image velocimetry (DPIV) (see Materials and methods). Scale bars (white, lower left) represent 1 cm; scale arrows (white, lower left) represent a flow speed of 25 cm s^{-1}. β, particle trajectory angle. Values are means ± S.D.

The swimming speed of $1.2\,FL\,s^{-1}$ is within the range of swimming speeds (0.4–3.5 body lengths s^{-1}) that mackerel can sustain for more than 200 min (He and Wardle, 1988) and matches a speed used in our previous studies (Nauen and Lauder, 2000; Nauen and Lauder, 2001). Speeds greater than $1.2\,FL\,s^{-1}$ were not used because, at higher speeds, the images were not suitable for analysis using particle-tracking methods. Note that, as the body of *Scomber japonicus* is extremely reflective, there is considerable glare in the image when mackerel directly intersect the light sheet (e.g. the areas on the lower left of the images in Fig. 2). Therefore, particles along the body were tracked just before and just after the body of the mackerel had directly intersected the light sheet. Considerable effort was expended to obtain video sequences during which the mackerel were swimming steadily (not drifting either vertically or laterally) and during which the orientation of the finlets and caudal peduncle relative to the laser light sheets was such that individual particles could be tracked reliably.

Reconstructing the flow

We recorded images of the left surface of the mackerel in the *xy* plane. Data from this view were used to reconstruct flow patterns over both sides of the peduncle because (i) the peduncle is bilaterally symmetrical, (ii) during steady swimming at a single speed, lateral movements of the body and caudal fin are similar (e.g. fig. 7 and fig. 5 in Nauen and Lauder, 2000) and (iii) both the leading and trailing surfaces of the peduncle can be seen from the left side of the fish at different points in the tailbeat cycle. The trailing surface of the peduncle (with the finlets at their maximum excursion in view of the camera, or ‘present’, along the left surface of the peduncle, Fig. 1A) was visible as the peduncle and caudal fin decelerated to the right. The leading surface of the peduncle (with the finlets not in view or ‘absent’ on the left surface of the peduncle, Fig. 1B) was visible as the peduncle and caudal fin decelerated to the left. The terms ‘leading surface’ and ‘trailing surface’ will be used to describe the peduncle in terms of its direction of movement relative to the video camera for the remainder of the paper. Similarly, the terms ‘present’ and ‘absent’ will be used to describe the position of the finlets relative to the left surface of the caudal peduncle.

Digital particle image velocimetry (DPIV)

Digital particle image velocimetry (DPIV) methods were used to determine the general trajectory of flow around the mackerel during the deceleration phase of the stroke. Video images were imported into a PC using DT-Acquire software with a Data Translation video card (Data Translation, Inc, USA). Using Insight software (version 3, TSI, Inc., USA), selected areas (e.g. Fig. 2) of sequential pairs of video images (4 ms apart) were analyzed by subdividing the area of interest of the images into a series of interrogation windows and comparing these data subsets using two-frame cross-correlation analysis. The areas of flow analyzed here were typically rectangular in shape (rather than the traditional square) because image area above and below the mackerel was limited (e.g. Fig. 2) as a result of the high level of magnification used to view the finlets.

The calculated velocity vectors were validated using Datashow (version 3, TSI, Inc., USA) in which a dynamic mean-value algorithm is used to reject any vectors in which the velocity of the vector was markedly higher than the average velocity of its eight nearest neighbors. The trajectories of the vectors were calculated trigonometrically from orthogonal velocity components using Transform (version 3.3, Fortner Research LLC, USA). For a more detailed discussion of DPIV, see Willert and Gharib (Willert and Gharib, 1991), Anderson (Anderson, 1996) and Raffel et al. (Raffel et al., 1998). For a more detailed description of the DPIV methods used here, see Drucker and Lauder (Drucker and Lauder, 1999), Lauder (Lauder, 2000) and Wilga and Lauder (Wilga and Lauder, 2000).

Vertical light sheet images were analyzed from the mackerel 24 cm in length. Horizontal light sheet images were analyzed from the mackerel 26 cm in length. At least ten pairs of images were analyzed for each view; representative data are presented here. Note that the horizontal light sheet images were selected relatively early in the deceleration phase (see, for example, Fig. 5) because since the field of view of the camera was relatively small and the lateral movement of the peduncle extended across the *z* axis of the field of view, in the later stages of deceleration the tail was too close to the bottom of the field of view for DPIV analysis along both sides of the body.

Particle-tracking analysis

DPIV methods cannot be used to analyze flow directly adjacent to a moving boundary, such as the body of a fish, because the analysis algorithms cannot differentiate between movement of the fish and movement of a particle, and analysis of areas of interrogation that contain moving surfaces (such as the fish) result in incorrect and very inaccurate calculations of flow for that area of the image (Willert and Gharib, 1991; Anderson, 1996; Raffel et al., 1998). Thus, a manual particle-tracking method was used to determine the movement of particles in close vicinity to the finlets and caudal peduncle (e.g. Fig. 3). The particle-tracking method also has the advantage of not requiring the relatively large calculation areas needed for DPIV, so data could be collected over all phases of the tail deceleration (see, for example, Fig. 7). Using a customized digitizing program, the positions of individual particles were digitized for a series of sequential frames as the peduncle decelerated to the left or the right. The origin of the digitizing coordinates was set to a fixed point on the caudal peduncle so that particle tracks from different strokes could be compared. In total, more than 800 particles were digitized.

The goal of the vertical light sheet analysis was to quantify the characteristics of flow along, above and below the body and finlets to test the effects of finlets 4 and 5 on flow trajectory and speed. We focused on posterior finlets 4 and 5 because these finlets have a potentially large hydrodynamic effect on flow in the region of the caudal fin. We compared the trajectory and speed of flow along the peduncle and finlets 4 and 5 (within

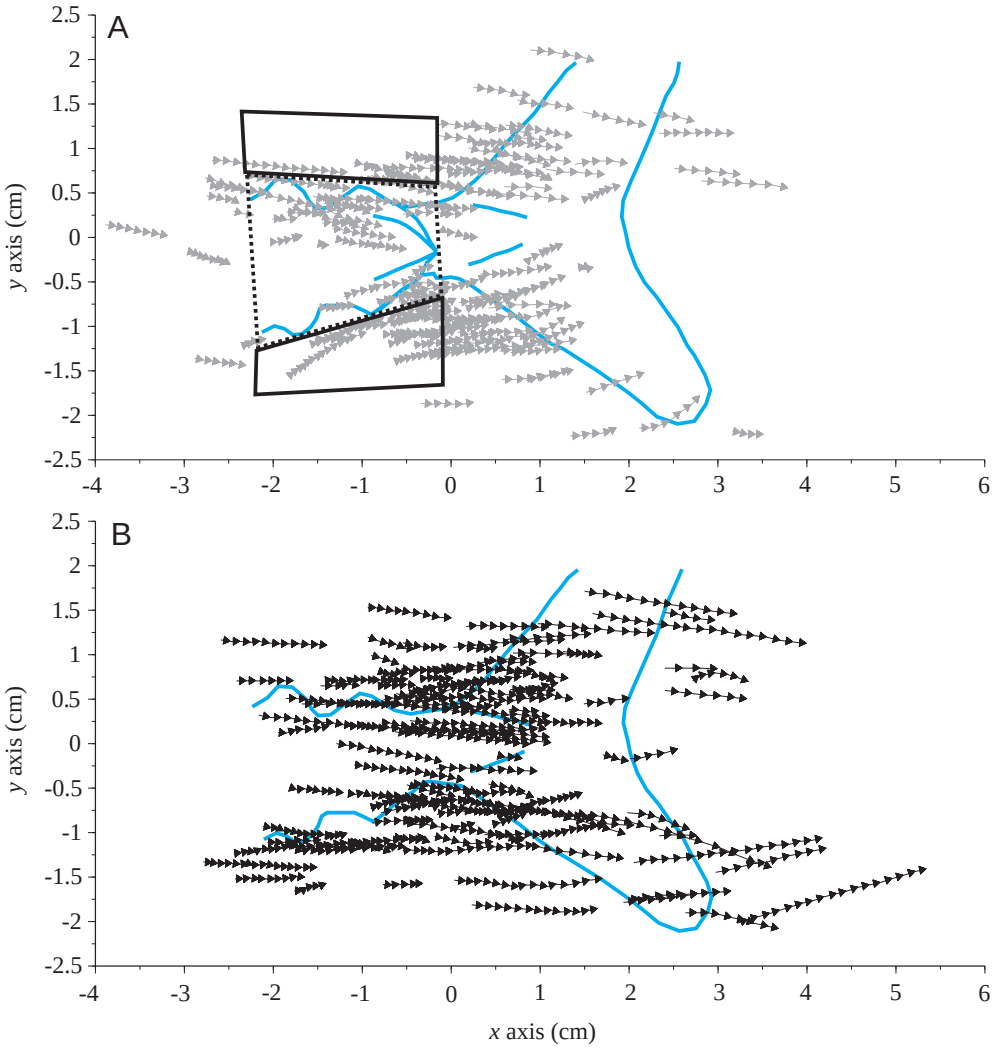

Fig. 3. Lateral view of particle tracks along the trailing (A, finlets present, gray particle tracks) and leading (B, finlets absent, black particle tracks) surface of the caudal peduncle and caudal fin (outlined in blue) as the peduncle decelerates during steady swimming at 1.2 *FL* s^{-1}, where *FL* is fork length. The caudal keels (blue lines) are shown on the lateral surface of the caudal fin. These particles were digitized from four consecutive tail strokes by a mackerel 24 cm in fork length. Each track represents the movement of a single particle; each arrow represents the distance traveled by that particle in 4 ms. Particle tracks along the finlets and caudal peduncle (within the dotted lines in A) were compared with the tracks of particles above and below the finlets and peduncle (within the solid lines in A) to describe flow in the region of and adjacent to the finlets and to test hypotheses about finlet function.

the dotted box of Fig. 3A) with flow immediately above and below these finlets (within the solid boxes of Fig. 3A) to avoid potentially confounding effects on the flow of the considerable tapering of the body posterior to the second dorsal fin and of the anterior three finlets.

Particles were randomly distributed in the flow, so the number of particles available for tracking in the vicinity of the peduncle or the finlet was related to the structure's surface area. Because of the relatively large lateral surface area of the body and the finlets (Fig. 3), 20 particles (10 above and 10 below the body midline) were tracked for each stroke in the vertical light sheet images over a series of at least three tailbeats (Fig. 3 shows these data for one of the four fish). The goal of the horizontal light sheet analysis was to determine the orientation of finlet 5 to the local flow. Because of the relatively small ventral surface area of the peduncle and finlets (see, for example, Fig. 5), we tracked at least 10 particles over a series of 2–4 strokes for each mackerel to analyze the trajectory of flow in the horizontal plane. To determine the angle of attack of the finlets, we also measured the orientation of the fifth finlet to the horizontal, and digitized the *xz* position of the body at the anterior base of finlet 5 as an index of axial body bending.

The unfiltered coordinate data were imported into Excel (Microsoft) to calculate particle speed and trajectory. The trajectory angle of the particle (β) in the *xy* plane was calculated relative to the horizontal as:

$$\arctan\beta = (y_t - y_{t-i})/(x_t - x_{t-i}), \quad (1)$$

where *t* is time and y_{t-i} or x_{t-i} is the position of the particle on the *y* or *x* axis, respectively, at time *t*–i. *z* was substituted for *y* in the above equation to calculate the trajectory angle of the particle in the *xz* plane relative to the *x* axis. Particle speed was calculated from the position data as:

$$S_t = (x_{t+i} - x_{t-i})/(2\Delta t), \quad (2)$$

where S_t is speed at time *t* (Winter, 1989). Calculating accurate speed values from digitized distance data is a complicated issue because of error inherent in the digitized data and variability in the equations used (as discussed by Harper and Blake, 1989; Biewener and Full, 1992; Walker, 1998). Note that, in our previous study (Nauen and Lauder, 2000), we determined that speed values calculated using the Winter equation (Winter, 1989) on data digitized using the methods described here are essentially identical to those calculated using the quintic spline

method in the Quicksand program that is generally recommended by Walker (Walker, 1998).

Statistical analyses

Statistical analyses were performed using Statgraphics (version 3.0 for Windows, STSC, USA). Regression relationships were compared using analysis of covariance (ANCOVA; Zar, 1984). The speeds of the particles on the leading and trailing surfaces of the peduncle were compared using a three-factor analysis of variance (ANOVA) in which individual was considered a random effect and the position of the particle above or below the body midline and the direction of peduncle movement were considered fixed effects. Particle trajectory data above and below the body midline were analyzed as separate three-factor ANOVAs (using the factors listed above) because the measurements were made relative to the lateral body midline. All F values were calculated as described by Zar (Zar, 1984).

Results

Flow in the vertical plane

DPIV calculations indicate that, viewed in the *xy* plane (Fig. 2), flow above and below the trailing surface of the peduncle was convergent as the peduncle decelerated and the finlets were positioned at maximum excursion along the peduncle's trailing surface. In the example shown in Fig. 2A, the mean trajectory angle (β) of flow vectors above the dorsal body surface and finlets calculated over a 4 ms time interval was −6±3° to the horizontal (mean ± S.D., N=30). The average β value below the ventral body surface and finlets was 10±5° (mean ± S.D., N=30). Thus, the trajectory of flow above and below the trailing surface of the peduncle was convergent. In contrast, during deceleration, flow trajectories above and below the leading surface of the peduncle (when the finlets were absent) were effectively horizontal (Fig. 2B), with mean β values of −1±0.5° (mean ± S.D., N=30) above and −1±0.4° (mean ± S.D., N=30) below the dorsal and ventral body surfaces and finlets, respectively (Fig. 2B).

Manual tracking of particles situated along and close to the body over a series of images indicated strong planar downstream flow because particles visible in the *xy* light sheet were frequently tracked for as long as 40 ms (Fig. 3A,B). The three-way analysis of variance (ANOVA) of particle speed (Table 1) as a function of individual, direction of peduncle movement and position of the particle (along the peduncle and finlets, such as the tracks within the dotted box in Fig. 3A, or above or below the finlets and caudal peduncle, such as the tracks within the solid boxes in Fig. 3A) indicated significant effects of individual (P=0.0009) and significant interaction effects of particle position×individual (P=0.0002), the direction of peduncle movement×individual (P=0.009) and the direction of peduncle movement×individual×particle position (P=0.0009). The significant effect of individual was expected because the mackerel, which were swimming at $1.2\,FL\,s^{-1}$, differed moderately in size (size range 20–24 cm FL for the vertical sheet images). There were no significant effects of the direction of peduncle movement (P=0.44, Table 1) or of the position of the particle relative to the caudal peduncle and finlets (P=0.73, Table 1) on particle speed. Thus, the finlets did not significantly affect flow speed. Mean particle speed estimates for these trajectories near the body for each of the four individuals, which were lower in magnitude than free-stream flow, ranged from 21±4 to 24±4 cm s^{-1} (means ± S.D., N>97 in all cases) for the four individuals. Averaged over the four individuals, particle speed was 23±4 cm s^{-1} (mean ± S.D., N=467).

Examination of the particle tracks from four consecutive strokes of a 24 cm mackerel suggests convergent flow along the trailing surface of the peduncle (Fig. 3A) and longitudinal

Table 1. *Results (*F *values) of the three-way ANOVA on particle speed during tail deceleration*

Variable	Individual	Presence of finlets/ direction of tail movement	Particle position§	Particle position × presence of finlets/ tail movement	Particle position × individual	Presence of finlets/ tail movement × individual	Presence of finlets/ tail movement × individual × particle position
d.f.	3, 451	1, 3	1, 3	1, 3	3, 451	3, 451	3, 451
Particle speed	5.6**	0.8	0.15	0.1	6.7**	3.9**	5.6**
Trajectory angle of particles below lateral body midline	7.6‡,**	24.7**	6.7	14.7**	0.1‡	1.7‡	1.0‡
Trajectory angle of particles above lateral body midline	15.8‡‡,**	40.1**	0.15	0.2	0.2‡‡	0.8‡‡	3.1‡‡,**

d.f., degrees of freedom.
§Along or above/below the finlets and caudal peduncle (see boxed regions in Fig. 3A).
**Statistically significant effect (P<0.05).
‡Residual d.f.=209; ‡‡residual d.f.=226.

or horizontal flow along the leading surface of the peduncle (Fig. 3B). The three-way ANOVA of the trajectory angles of particles situated below the body midline as a function of the same three factors considered for particle speed (Table 1) indicated significant effects of individual (P=0.0001) and the direction of peduncle movement (P=0.02) and significant interaction effects of particle position×direction of peduncle movement (P=0.03). There were no significant effects of the position of the particle relative to the finlets and caudal peduncle (P=0.081) and no other significant interaction effects (Table 1). Thus, the position of the ventral finlets did not affect the trajectory of flow below the lateral midline of the body. The three-way ANOVA of the trajectory angles of particles situated above the body midline (Table 1) as a function of the same three factors indicated significant effects of individual (P=0.0001) and the direction of peduncle movement (P=0.008) and significant interaction effects of particle position×direction of peduncle movement×individual (P=0.03). The position of the particle relative to the finlets and caudal peduncle (P=0.72) and the other interaction effects were not significant (Table 1). Thus, the position of the ventral finlets did not affect the trajectory of flow above the lateral midline of the body. The data indicate that, in the vertical plane, particle trajectory was dependent on the direction of peduncle movement and not on the position of the finlets.

Plotting mean values of the angle of individual particles to the horizontal as a function of the mean values of the vertical position of these particles on the body (Fig. 4A) supports the finding that flow trajectory is dependent on the direction of peduncle movement. When the peduncle and caudal fin are beating to the right (allowing visualization of the trailing peduncular surface) and the finlets are present (Fig. 4A, gray symbols), the linear regression model shows a slope of −14 (P<0.0001), indicating the creation of strong convergent flow. When the peduncle and caudal fin are beating to the left (allowing visualization of the leading peduncular surface) and the finlets are on the other side of the body (Fig. 4A, black symbols), the trajectories of the particles are close to horizontal, with a low but statistically significant slope of −3 (P<0.0001). The slopes of the regression models shown in Fig. 4A are significantly different (ANOVA, P=0.0001).

A second way to illustrate the statistical finding that in the

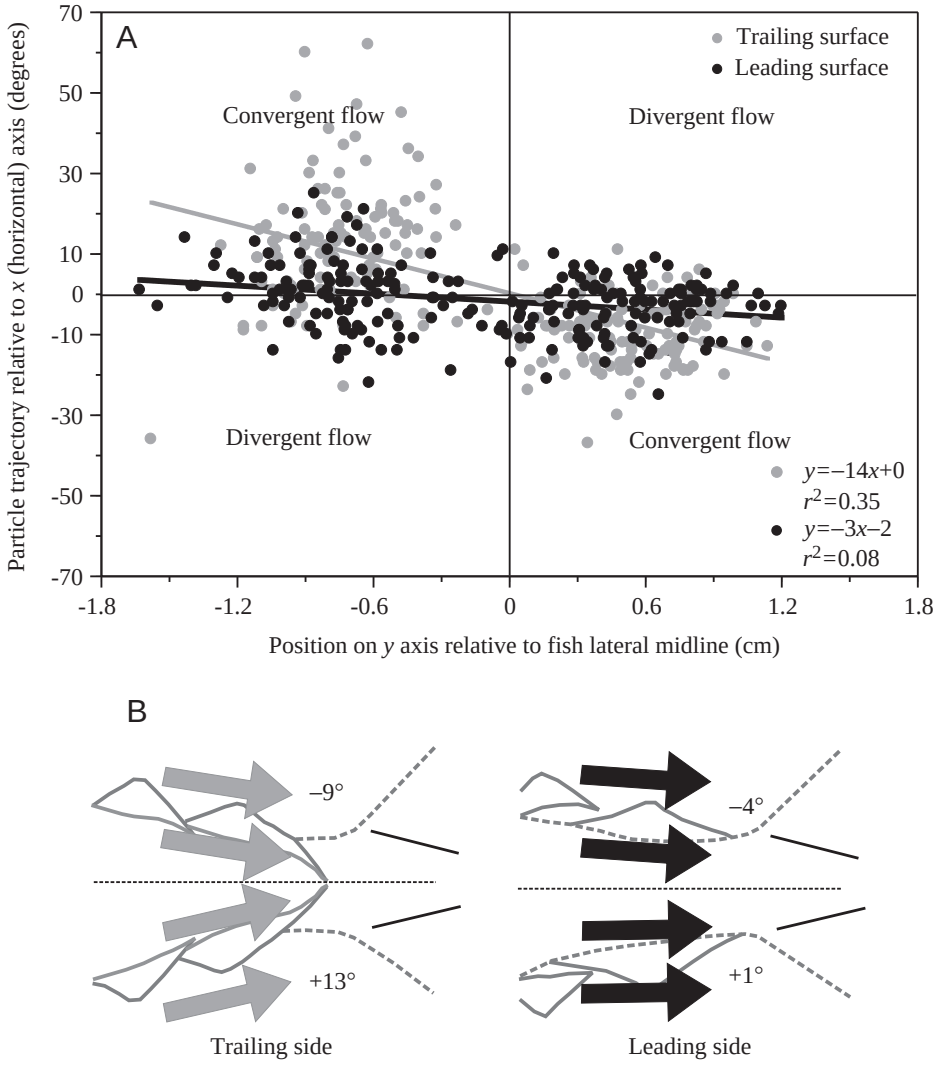

Fig. 4. Particle trajectory along the trailing (gray circles, finlets present) and leading (black circles, finlets absent) lateral surfaces of the caudal peduncle as a function of the vertical position of the particle on the body (A) for all four mackerel examined. Each symbol represents a single particle; mean trajectory and position (N=3 or more) for each particle are plotted here. The lines represent the linear regression models fitted to the data sets. Note that the abscissa of this panel indicates the position of each point relative to the y axis (see Fig. 1), with positive and negative values indicating dorsal and ventral locations relative to the horizontal midline, respectively. The ordinate indicates the angular trajectory of each particle track. These data are summarized graphically in B, in which a lateral view of the caudal peduncle (gray dashed lines), finlets 4 and 5 (gray solid lines), the lateral body midline (black dotted line) and the caudal keels (black lines) is depicted. Average values of flow trajectory (arrows) along the caudal peduncles and finlets and above and below these structures are shown on the trailing (gray arrows) and leading (black arrows) surface of the peduncle.

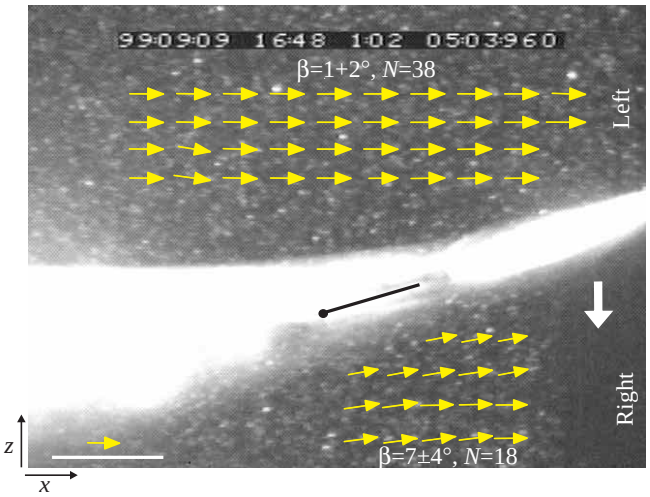

Fig. 5. Ventral view of a 26 cm fork length (*FL*) mackerel swimming at 1.2 *FL* s^{-1} illuminated by a laser light sheet oriented in the horizontal (*xz*) plane. The peduncle and caudal fin are beginning to decelerate to the right (direction indicated by white arrow). The ventral margin of finlet 5 is outlined by the black line; its anterior attachment point is indicated by the black circle. Flow vectors were calculated using digital particle image velocimetry (DPIV); mean values of flow trajectory (β) indicate the formation of cross-peduncular flow on the right side of the mackerel and longitudinal flow on the left side of the mackerel. Values are means ± S.D. The scale bar (white, lower left) represents 1 cm (note that only the posterior fifth of the body is seen in the field of view); the scale arrow (white, lower left) represents a flow of 25 cm s^{-1}.

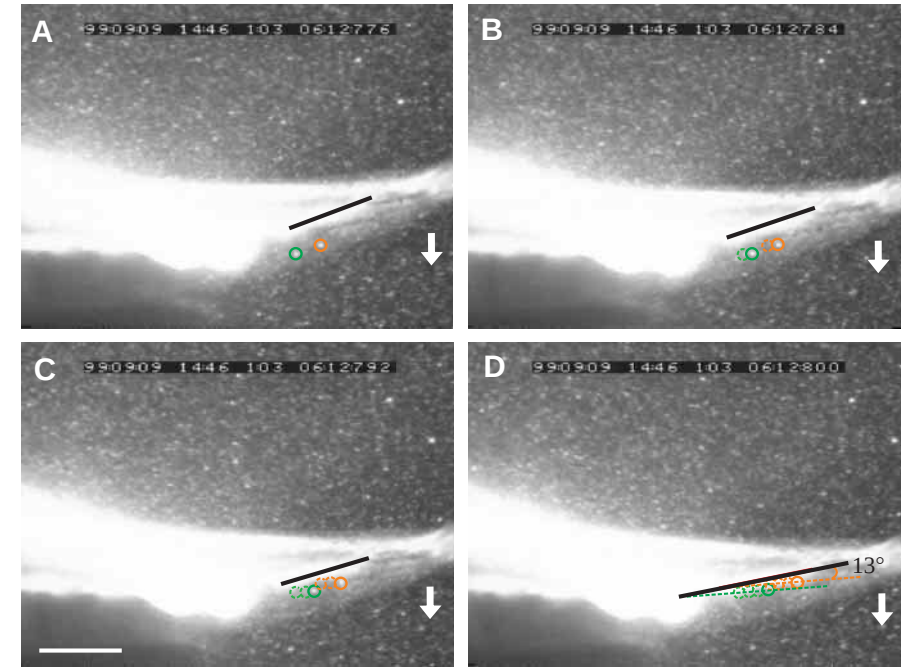

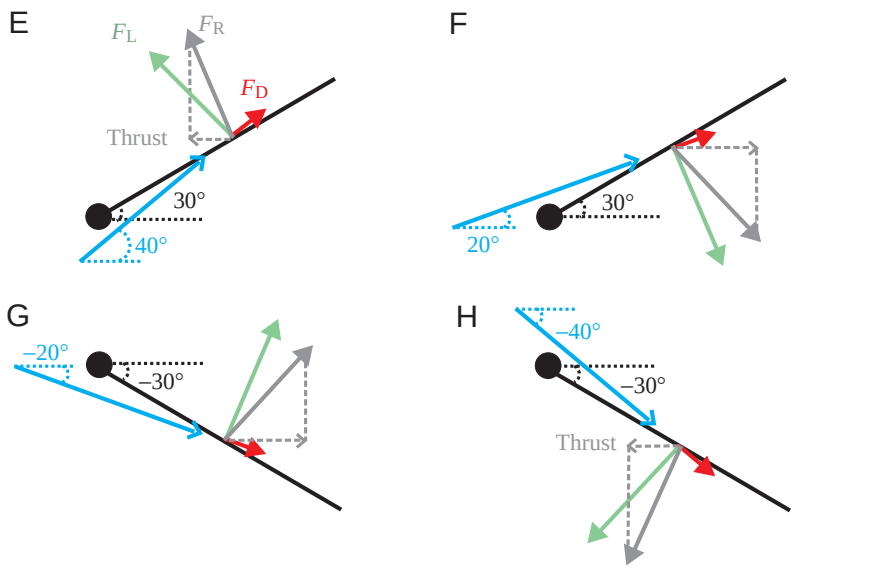

Fig. 6. The position of two particles (highlighted by the green and orange open circles) are tracked through a time series of images (A–D) showing the ventral view of a 26 cm fork length (*FL*) mackerel swimming at 1.2 *FL* s^{-1} as the peduncle declerates to the right (direction of movement indicated by the white arrow). The ventral surface of the mackerel and reflective particles in the water are illuminated by a laser light sheet oriented in the horizontal plane. The ventral margin of the fifth finlet is highlighted by the black line. The scale bar (white line, lower left of C) represents 1 cm. (E–H) Diagrams presenting hypothetical lift (F_L, green arrows), drag (F_D, red arrows) and resultant forces (F_R, gray arrows) created by the interaction between a finlet (solid black lines) and the local flow (solid blue lines) of varying trajectories. The orientations of the finlet and flow with respect to the horizontal are indicated by dotted black and blue lines, respectively. Note that thrust, which in these cases is produced when the resultant vector is angled to the left, is created only if the angle between the finlet and the horizontal is less than that of the local flow (E and H). Data shown in A–D correspond to the theoretical diagram in F, in which no thrust is generated.

vertical plane particle trajectory was dependent on the direction of peduncle movement, and not on the movement of the finlets, is to compare the mean values of particle trajectory along the leading and trailing surfaces of the peduncle (Fig. 4B). Along the trailing surface of the peduncle, the mean trajectory angle of the particles relative to the horizontal was 13±15° (mean ± S.D., *N*=111) below the body midline and –9±8° (mean ± S.D., *N*=124) above the body midline. Thus, on average, the flow trajectory along the trailing surface of the peduncle was convergent during peduncle deceleration. Along the leading surface of the peduncle, the average trajectory of the particles was 1±9° (mean ± S.D., *N*=114) below the body midline and –4±7° (mean ± S.D., *N*=118) above the body midline as the peduncle decelerated. Thus, on average, the trajectory of flow along the leading surface of the peduncle was close to horizontal during peduncle deceleration (Fig. 4B). The flow trajectory was independent of finlet movement, however, because on both the leading and trailing sides of the peduncle the trajectories of particles immediately above and below the finlets were not significantly different from those of particles along the finlets and peduncle (Fig. 4B; Table 1). Thus, the particle-tracking data indicate that during the second half of each stroke movement of the body, and not of the finlets, determines the trajectory of flow along the finlets and caudal peduncle in the vertical plane.

Flow in the horizontal plane

DPIV measurements in the *xz* plane indicate that, as the peduncle is decelerating to the right, flow to the left of the mackerel has a longitudinal trajectory while flow to the right of the mackerel is angled towards the mackerel. In the example shown in Fig. 5, flow to the left of the mackerel has a trajectory (β) value of 1±2° (mean ± S.D., *N*=38) and flow to the right has a β value of 7±4° (mean ± S.D., *N*=18).

The goal of horizontal light sheet analysis was to determine the orientation of finlet 5 to the trajectory of local flow during deceleration of the peduncle. Following the movement of individual particles over time (e.g. Fig. 6A–D) indicated that particle trajectory was not parallel to finlet orientation. In the example shown in Fig. 6, finlet 5 is at a larger angle to the horizontal than the two particles that were tracked, indicating that finlet 5 is at a negative angle of attack to the local flow (corresponding to Fig. 6F). A times series of the orientation of finlet 5 and the trajectory of local flow for a mackerel 24 cm in length is presented in Fig. 7. The orientation of finlet 5 to the horizontal, the lateral movement of the body and the trajectory of numerous particles close to finlet 5 are plotted over a series of five continuous strokes (Fig. 7). The data show that, as the peduncle decelerates during the second half of each stroke, finlet 5 (black symbols, Fig. 7) is consistently at a larger angle to the horizontal than is the local flow (colored symbols,

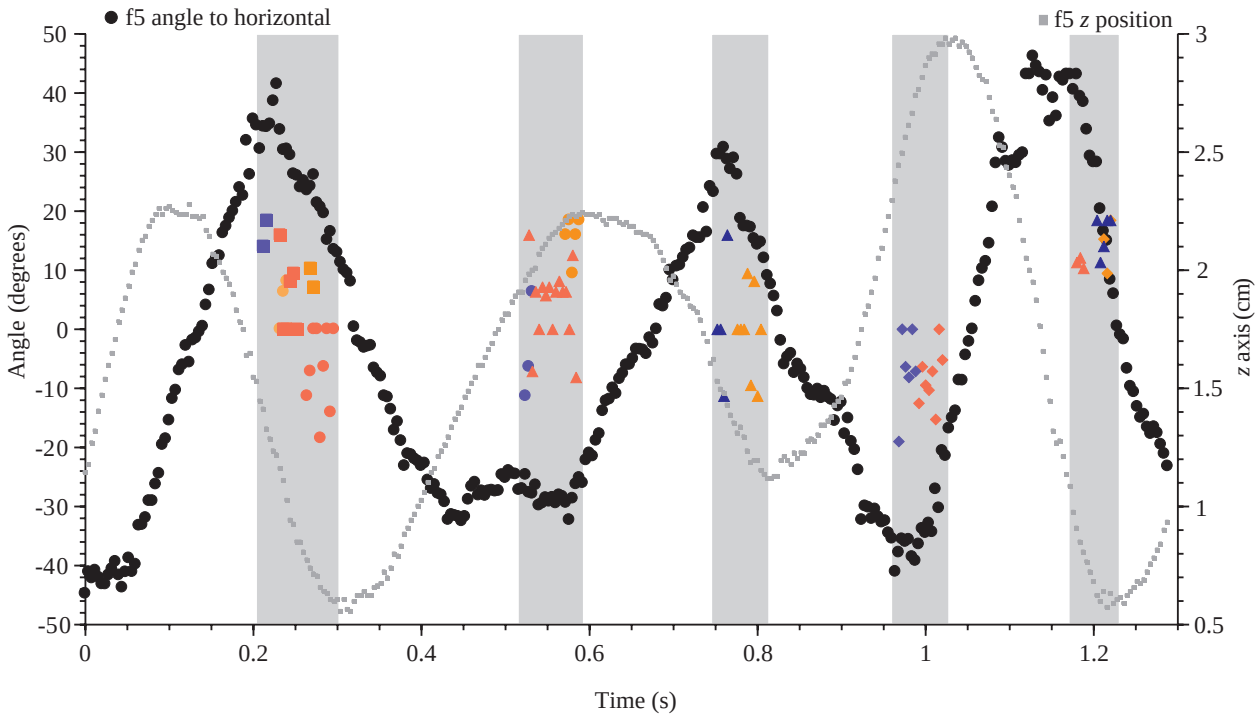

Fig. 7. A time series of the angle of finlet 5 (f5; black symbols) and the angles of various particles (each particle in a stroke is represented by a different colored symbol) with respect to the horizontal (left *y* axis) over a series of five strokes. The oscillation of the body of the 24 cm mackerel swimming at 1.2 *FL* s^{-1}, where *FL* is fork length, is represented by the position of the body at the insertion of finlet 5 on the *z* axis (gray symbols, right *y* axis). Particles were digitized over the second half of each stroke (at times highlighted by the gray boxes), during which time the peduncle and caudal fin decelerate (Nauen and Lauder, 2000). Note that the particle trajectory angles are not equal to the orientation angle of finlet 5 over a series of strokes, indicating that finlet 5 is at an angle of attack to the local flow and that the finlet is typically oriented at a steeper angle to the horizontal than is the local flow, indicating that no thrust is produced (see Fig. 6F,G).

Fig. 7). This orientation corresponds to Fig. 6F and Fig. 6G, which indicates that finlet orientation to the local flow does not result in thrust production from lift generation. The differences between particle trajectory and finlet orientation are consistent for particles tracked for 3–15 video images (highlighted regions, Fig. 7) despite the changes in finlet orientation and peduncle position over that time. Note that, for the five complete strokes quantified here, the mean lateral undulation of the caudal peduncle is 1.8±0.5 cm (mean ± S.D., N=5) or approximately 7 % of body length.

To examine the relationship between flow trajectory and finlet orientation more closely, data for four mackerel are plotted in Fig. 8. Mean values of particle trajectory are plotted as a function of mean finlet 5 orientation values because of the consistent relationship between the variables in the time series data (Fig. 7). Data from the four individuals are plotted together in Fig. 8 because the slopes and y-intercepts for linear regression relationships fitted to the data sets for individual mackerel were not significantly different (ANOVA, P=0.24 and P=0.15, respectively). If the trajectories of particles close to the finlet were parallel to the orientation of the finlet, one would expect a 1:1 relationship between particle trajectory angle and finlet angle (dashed line in Fig. 8). The slope of 0.26 of the linear regression relationship fitted to the grouped data is significantly different from zero (t-test, P<0.001) and significantly different from the predicted slope of 1 (P<0.0001). The positive slope of the regression relationship indicates that the angle of attack of finlet 5 varied as a function of particle trajectory angle from values of zero to up to values of approximately 40 °. The mean angle of attack for the data shown in Fig. 8 is 18±13 ° (mean ± S.D., N=45). Thus, finlet 5 is frequently at a relatively high angle of attack to the local flow as the peduncle decelerates during the second half of each stroke. The orientation of finlet 5 to the local flow does not result in thrust production from lift generation (see Fig. 6F,G); however, the fact that finlet 5 is not parallel to the local flow indicates that this finlet redirects flow during the deceleratory phase of the stroke. Analysis of a more limited data set during acceleration of the peduncle indicated similar results.

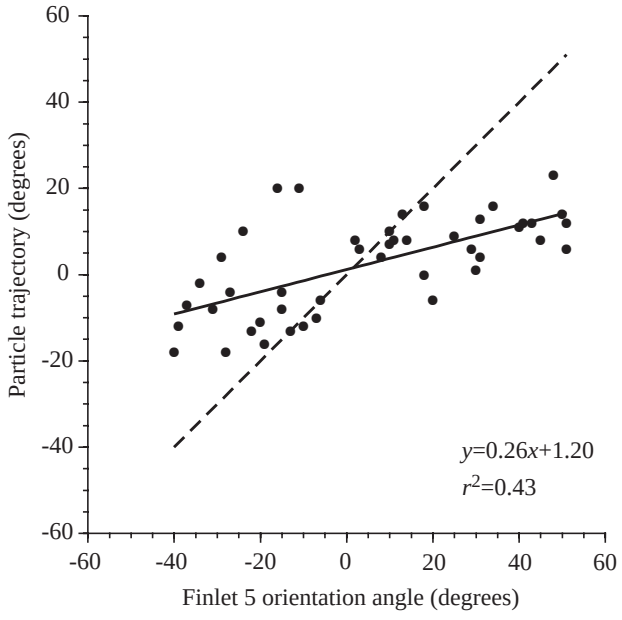

Fig. 8. Particle trajectory angle as a function of the angle of finlet 5. Each symbol represents the mean angle (N=3 or more) for a single particle. The broken line represents a 1:1 relationship. The solid line represents the least-squares linear regression relationship fitted to the mean data.

Discussion

General water flow patterns over the peduncle

Images of vorticity formed along the body of a swimming fish and subsequently shed into a wake, such as those of Blickhan et al. (Blickhan et al., 1992), Anderson (Anderson, 1996), Muller et al. (Muller et al., 1997), Videler et al. (Videler et al., 1999) and Wolfgang et al. (Wolfgang et al., 1999), form the basis for the view that upstream flow and vorticity along the body interact with vortices produced at the caudal fin to increase force output during swimming. Indeed, Wolfgang et al. (Wolfgang et al., 1999) concluded that the tail is secondary in the creation of wake vortices because vorticity is generated far upstream of the tail by undulations of the body and is then enhanced and shed by the movement of the caudal fin.

The recent comparative study of boundary layer formation in dogfish (*Mustelus canis*) and scup (*Stenotomus chrysops*) (Anderson et al., 2000) suggests that the relative importance of the body *versus* the caudal fin in generating vorticity (and therefore force) is dependent on morphological and kinematic variables. Mean streamwise acceleration in the boundary layer, which is a sign of thrust production (Anderson et al., 2000), was relatively low in the scup compared with the dogfish. Anderson et al. (Anderson et al., 2000) interpreted this result as reflective of relatively low levels of 'body-based thrust' produced by the scup compared with the dogfish because of kinematic differences between the two fish.

The study of Anderson et al. (Anderson et al., 2000) indicates that more data need to be collected before the relative contribution of the body *versus* the tail in the generation of vorticity is clearly understood. Nonetheless, these previous studies have demonstrated the importance of characterizing flow along the body and the interaction between this flow and the caudal fin to understand the hydrodynamics of fish axial propulsion. The data presented here contribute to this emerging picture of flow over the body of swimming fish and reveal an interesting pattern of flow around the caudal peduncle and finlets of *Scomber japonicus*.

At the relatively slow swimming speed of 1.2 $FL\,s^{-1}$, DPIV analysis in the xy plane indicated that, during the deceleratory phase of the stroke, flow above and below the mackerel's body had different trajectories on the leading and trailing surfaces of the peduncle. Above and below the leading surface of the peduncle, flow trajectory was essentially 0 ° (relative to the horizontal). In contrast, above and below the trailing surface of the peduncle, flow trajectory was convergent, with average

β values of –6 ° above the body and 10 ° below the body. Flow along the caudal peduncle and finlets showed the same pattern: flow was close to horizontal (on average, –4 ° above the body midline and 1 ° below the body midline) on the leading surface of the peduncle and convergent (–9 ° above the body midline and +13 ° below the body midline) on the trailing surface of the peduncle. Thus, the vertical light sheet data indicate that there are different flow trajectories on the leading and trailing surfaces of the peduncle as the tail is decelerating.

We propose that this flow field is created by a combination of the lateral movement of the peduncle through the water and flow moving down the body. If mackerel were gliding straight ahead, and thus not showing lateral body movement, one would predict flow converging posteriorly on both surfaces of the caudal peduncle because of the streamlined fusiform body shape (Fig. 9A). Liu et al. (Liu et al., 1997) computationally predicted such convergent flow for a non-undulating tadpole (5 cm in length), although the body of the tadpole is more gibbous in shape than the mackerel studied here.

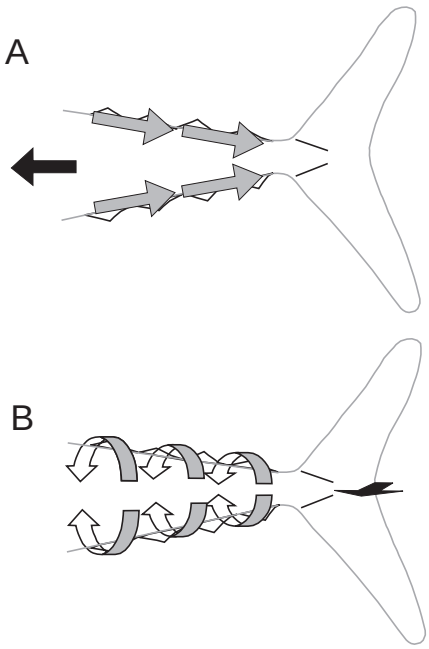

Fig. 9. Schematic lateral view of the left side of a chub mackerel in which the body is outlined in gray and the finlets and caudal keels are outlined in black. Idealized flow trajectories (gray arrows) are shown for forward gliding (A, body motion indicated by the black arrow), in which there is no lateral movement of the caudal peduncle or finlets, and for lateral movement of the body without forward movement (B, body motion indicated by the black arrow). Forward gliding without lateral movement (A) is expected to create convergent flow along the peduncle. Lateral movement of the peduncle without forward movement (B) is expected to create divergent flow on the leading surface of the peduncle and convergent flow on the trailing surface. The observed flow pattern on a steadily swimming mackerel is a combination of these two idealized patterns. Above the lateral midline of the fish on the leading peduncular surface (shown), the downward trajectory of flow above the horizontal expected under A sums with the upward trajectory expected under B to result in essentially horizontal flow. The downward trajectory of flow on the trailing peduncular surface expected under A sums with the downward trajectory expected under B to result in flow above the horizontal moving towards the midline on the trailing surface. Flow below the horizontal follows the opposite pattern.

Convergent flow formed by the forward movement of the body would merge with lateral flow formed by the lateral motion of the body during steady swimming (Fig. 9B). Lateral motion of the body of *Scomber japonicus* is largely restricted to the posterior finlets, caudal peduncle and caudal fin in the carangiform swimming mode (Lindsey, 1978; Videler and Hess, 1984; Donley and Dickson, 2000). The amplitude of lateral oscillation increases rapidly over a relatively small region of the body, the caudal peduncle (Lighthill, 1975; Lindsey, 1978). The caudal peduncle accelerates and decelerates laterally with each stroke (for an example of this pattern for mackerel swimming at $2.2\,FL\,s^{-1}$, see fig. 11 in Nauen and Lauder, 2000). For the 24 cm mackerel observed here swimming at $1.2\,FL\,s^{-1}$, the oscillation amplitude of the caudal peduncle is approximately 7±2 % of fork length (mean ± S.D., N=5). Thus, at a speed of $1.2\,FL\,s^{-1}$, there is appreciable lateral movement of the peduncle at the longitudinal location of the fifth finlet. Measurements of *S. japonicus* of similar size swimming at the same speed (relative to body length) indicated that lateral movement of the body increases to an average of 11 % of body length at the anterior margin of the caudal fin on the body and 14 % of body length at the tip of the caudal fin (calculated from table 2 of Gibb et al., 1999), demonstrating the posterior increase in lateral oscillation, with the largest excursions over the caudal fin, that is typical of carangiform locomotion (Lighthill, 1975).

As the peduncle moves laterally through the water, it is to be expected that, like any bluff body in a fluid, water will flow from the leading to the trailing surface (Fig. 9B). We therefore expected to see diverging flow on the leading, high-pressure surface and converging flow on the trailing, low-pressure surface. Lighthill (Lighthill, 1960) modeled such a flow mathematically using three-dimensional elongated body theory (see the discussion of that model in Anderson, 1996). In the present study, converging flow was visualized along the trailing surface of the peduncle and above and below it. Lateral flow associated with lateral movement of the peduncle was visible in horizontal light-sheet DPIV and particle-tracking data; however, diverging flow was not seen on the leading surface of the peduncle. Flow trajectories were close to 0 ° with essentially no y-component of velocity on the leading surface of the peduncle, indicating that flow was moving only in the downstream direction.

The absence of diverging flow on the leading surface of the caudal peduncle was an unexpected observation that may be associated with the shape of the caudal peduncle of *Scomber japonicus*. As discussed by Lighthill (Lighthill, 1975), any lateral flow over the caudal peduncle is associated with local lateral forces. One way to minimize flow (and thus those forces) is to decrease the depth of the body where the

magnitude of lateral oscillation increases from small to large values (the peduncle, in the case of *Scomber japonicus*). Lighthill (p. 24 in Lighthill, 1975) used this reasoning to explain the narrowing or 'necking' of the caudal peduncle in scombrid fishes. Thus, the absence of diverging flow on the leading surface of the peduncle may partially be caused by the narrow profile of the caudal peduncle of *S. japonicus* that is characteristic of scombrid fish. Testing this hypothesis requires comparative flow-visualization experiments on a fish that has a forked caudal fin and on a fish that has a relatively thick peduncle, such as *Pomatomus saltatrix* (the bluefish), to determine the effect of the height of the peduncle (relative to the height of the body and caudal fin) on flow trajectory.

A second factor in the flow patterns seen here is the contribution of longitudinal flow moving down the body to the flow field at the caudal peduncle. As discussed previously, one would predict flow moving posteriorly along the mackerel to converge along both sides of the caudal peduncle because of the fusiform body shape of the fish. Lateral movement of the peduncle would create divergent flow on the leading surface of the peduncle and convergent flow on the trailing surface. Flow created by lateral movement of the peduncle would add to (and therefore strengthen) convergent flow along the trailing surface of the peduncle and interfere with (and therefore weaken) convergent flow along the leading surface of the peduncle (Fig. 9). Thus ,the pattern of horizontal flow over the leading surface of the peduncle and convergent flow over the trailing surface of the peduncle is consistent with the interaction between flow moving down the body and flow formed by lateral movement of the peduncle.

A final factor in the patterns of flow described here is the kinematics of the caudal peduncle and fin. Gibb et al. (Gibb et al., 1999) determined that, during steady swimming at $1.2\,FL\,s^{-1}$, the caudal peduncle and fin of *Scomber japonicus* are tilted at approximately 10° from normal to the *xz* plane in a similar manner to the homocercal caudal fin of other teleosts (Lauder, 2000). The present DPIV and particle-tracking data on the trailing surface of the peduncle indicate some flow asymmetry because, on average, the flow moving across the ventral surface of the peduncle had larger trajectory angles than the flow moving across the dorsal surface. This difference in trajectory may be, in part, the result of the asymmetrical movement of the caudal peduncle and fin, as observed by Gibb et al. (Gibb et al., 1999).

Hydrodynamic function of the finlets

As the summed surface area of the finlets is approximately 15% of caudal fin area (Nauen and Lauder, 2000) and the finlets are positioned immediately anterior to the caudal fin, it has been suggested that the finlets are locomotory structures. Walters (Walters, 1962), Lindsey (Lindsey, 1978) and Magnuson (Magnuson, 1970) all proposed that the finlets deflect water longitudinally. Kinematic data collected using two-dimensional (Nauen and Lauder, 2000) and three-dimensional (Nauen and Lauder, 2001) methods indicated that, during steady swimming at speeds of $1.2–3\,FL\,s^{-1}$, the finlets reach maximum excursion during deceleration and that the positions of finlets 4 and 5 at that time in the stroke are consistent with the convergent direction of flow along the trailing surface of the caudal peduncle and into the vortex forming at the caudal fin (the vorticity enhancement hypothesis). The present vertical light sheet data indicate, however, that convergent flow along the trailing surface of the caudal peduncle and finlets during deceleration is not significantly different from flow immediately above and below the finlets. The convergent flow along the peduncle is, therefore, relatively large-scale and not attributable to finlet movement. In terms of the redirection of flow in the vertical plane, hypotheses concerning vorticity enhancement and the redirection of flow longitudinally are not supported.

The present study suggests, however, that there is redirection of cross-peduncular flow by the finlets in the horizontal plane, supporting the hypotheses of Walters (Walters, 1962), Lindsey (Lindsey, 1978) and Webb (Webb, 1975). Our direct tracking of flow local to the finlets shows that finlet 5 is frequently at an angle of attack (α) of 10–20° to its local flow as the peduncle is decelerating (not 0° as previously calculated on the basis of two-dimensional kinematic data alone; Nauen and Lauder, 2000). Although finlet 5 is at an angle to the local flow, its orientation is not likely to result in the production of thrust from lift generation. The angle of attack of finlet 5 relative to the local flow is such that the resultant from lift and drag forces opposes the direction of motion (Fig. 6F,G) and, hence, finlet 5 is predicted to generate a drag (von Kármán) wake. These results contrast with our previous determination of angle of attack based on kinematic data alone (Nauen and Lauder, 2000) and underscore the importance of directly measuring fluid flow to determine angle of attack for biological airfoils undergoing complex movements, rather than assuming that flow is parallel to the path of motion.

Finlet 5 does redirect local flow, however, and it is likely that it sheds small vortices. Any vortices formed were not visible in the present experiments, so their orientation and potential interaction with the developing caudal fin vortices (Anderson, 1996) could not be determined. Nonetheless, the horizontal sheet data suggest that finlet 5 contributes to forming the flow field around the caudal fin of swimming mackerel during the deceleratory phase of the stroke. These data are the first direct demonstration that scombrid finlets have a hydrodynamic effect on local flow during steady swimming.

The position of the fifth finlet at an angle of attack to the local flow during steady swimming may be the result of passive movement, active movement or a combination of the two. Small muscles insert on the base of each finlet, and when mackerel glide at speeds of approximately $1\,FL\,s^{-1}$ individual finlets can move independent of both movement of the body and movement of the other finlets, which suggests active control of finlet position (Nauen and Lauder, 2000). During steady swimming, the phase and amplitude of finlet movement are independent of speed for speeds from 1.2 to $3\,FL\,s^{-1}$, however, which suggests that during steady swimming finlet movement is largely passive.

Hydrodynamic effects of the caudal keels

The presence of a pair of small, obliquely oriented keels on the lateral surface of the caudal fin is characteristic of the family Scombridae (Collette and Nauen, 1983). The more derived scombrid species also have a predominant central keel. The central keel is visible beneath the skin in cleared and stained specimens of *Scomber japonicus* but it does not project above the body surface (Nauen and Lauder, 2000). The lateral keels of *S. japonicus* are visible as small ridges on the outer surface of the fish and consist of a series of obliquely oriented, short, fine, bony elements that are possibly modified scales (Nauen and Lauder, 2000). The dorsal and ventral lateral keels of the four fish examined here are oriented at −14±1° (mean ± S.D., N=4) and 12±1° (mean ± S.D., N=4) relative to the horizontal, respectively. These values are very similar to the β values of −9° and 13° determined for the flow over the peduncle and finlets in the vertical plane. The trajectory of flow anterior to the keels is very similar to the orientation of the keels, so the lateral keels of *S. japonicus* are not redirecting flow towards the lateral midline of the caudal fin. We lacked sufficient flow data in the region of the keels to test the hypothesis that flow between the keels may accelerate, as proposed by Walters (Walters, 1962) and discussed by Lindsey (Lindsey, 1978). Given the small height (of the order of less than 1 mm) of the keels of *S. japonicus* (Nauen and Lauder, 2000), however, it is likely that the keels are positioned largely within boundary layer flow and, thus, have a limited effect on the speed of local flow.

The authors thank Laura Farrell for her careful and persistent digitizing, Ellen Freund for her suggestions on data interpretation and Cheryl Wilga for assistance with obtaining the mackerel for this study. We also thank Laura Farrell, Cheryl Wilga, Jimmy Liao, Eric Tytell and Tonia Hsieh for useful comments during the course of this project and two anonymous reviewers for helpful comments. Support was provided by NSF grant 9807021 to G.V.L.

References

Anderson, E. J., McGillis, W. R. and Grosenbaugh, M. A. (2000). The boundary layer of swimming fish. *J. Exp. Biol.* **204**, 81–102.

Anderson, J. M. (1996). Vorticity control for efficient propulsion. PhD thesis, Massachusetts Institute of Technology and the Woods Hole Oceanographic Institution, USA.

Biewener, A. A. and Full, R. J. (1992). Force platform and kinematic analysis. In *Biomechanics (Structures and Systems): A Practical Approach* (ed. A. A. Biewener), pp. 45–73. Oxford: Oxford University Press.

Blickhan, R., Krick, C., Zehren, D. and Nachtigall, W. (1992). Generation of a vortex chain in the wake of a subundulatory swimming. *Naturwissenschaften* **79**, 220–221.

Collette, B. B. and Nauen, C. E. (1983). *Scombrids of the World*. Rome: Food and Agriculture Organization of the United Nations.

Donley, J. M. and Dickson, K. A. (2000). Swimming kinematics of juvenile kawakawa tuna (*Euthynnus affinis*) and chub mackerel (*Scomber japonicus*). *J. Exp. Biol.* **203**, 3103–3116.

Drucker, E. G. and Lauder, G. V. (1999). Locomotor forces on a swimming fish: three-dimensional vortex wake dynamics quantified using digital particle image velocimetry. *J. Exp. Biol.* **202**, 2393–2412.

Drucker, E. G. and Lauder, G. V. (2000). A hydrodynamic analysis of fish swimming speed: wake structure and locomotory force in slow and fast labriform swimmers. *J. Exp. Biol.* **203**, 2379–2393.

Gibb, A. C., Dickson, K. A. and Lauder, G. V. (1999). Tail kinematics of the chub mackerel *Scomber japonicus*: testing the homocercal tail model of fish propulsion. *J. Exp. Biol.* **202**, 2433–2447.

Harper, D. G. and Blake, R. W. (1989). On the error involved in high-speed film when used to evaluate maximum accelerations of fish. *Can. J. Zool.* **67**, 1929–1936.

He, P. and Wardle, C. S. (1988). Endurance at intermediate swimming speeds of Atlantic mackerel, *Scomber scombrus* L., herring, *Clupea harengus* L. and saithe, *Pollachius virens* L. *J. Fish Biol.* **33**, 255–266.

Jayne, B. C., Lozada, A. F. and Lauder, G. V. (1996). Function of the dorsal fin in bluegill sunfish: motor patterns during four distinct locomotor behaviors. *J. Morph.* **228**, 307–326.

Knower, A. T. and Shadwick, R. E. (1999). Red muscle activation patterns in yellowfin (*Thunnus albacares*) and skipjack (*Katsuwonus pelamis*) tunas during steady swimming. *J. Exp. Biol.* **202**, 2127–2138.

Lauder, G. V. (2000). Function of the caudal fin during locomotion in fishes: kinematics, flow visualization and evolutionary patterns. *Am. Zool.* **40**, 101–122.

Lighthill, M. J. (1960). Note on the swimming of a slender fish. *J. Fluid Mech.* **9**, 305–317.

Lighthill, M. J. (1975). *Mathematical Biofluiddynamics*. Philadelphia: Society for Industrial and Applied Mathematics.

Lindsey, C. C. (1978). Form, function and locomotory habits in fish. In *Fish Physiology*, vol. VII, *Locomotion* (ed. W. S. Hoar and D. J. Randall), pp. 1–100. New York: Academic Press.

Liu, H., Wassersug, R. and Kawachi, K. (1997). The three-dimensional hydrodynamics of tadpole locomotion. *J. Exp. Biol.* **200**, 2807–2819.

Magnuson, J. J. (1970). Hydrostatic equilibrium of *Euthynnus affinis*, a pelagic teleost without a gas bladder. *Copeia* **1**, 56–85.

Muller, U. K., Heuvel, B. L. E. V. D., Stamhuis, E. J. and Vidler, J. J. (1997). Fish foot prints: morphology and energetics of the wake behind a continuously swimming mullet (*Chelon labrosus* Risso). *J. Exp. Biol.* **200**, 2893–2906.

Nauen, J. C. and Lauder, G. V. (2000). Locomotion in scombrid fishes: morphology and kinematics of the finlets of the chub mackerel *Scomber japonicus*. *J. Exp. Biol.* **203**, 2247–2259.

Nauen, J. C. and Lauder, G. V. (2001). A three-dimensional analysis of finlet kinematics in the chub mackerel (*Scomber japonicus*). *Biol. Bull.* **200**, 9–19.

Raffel, M., Willert, C. and Kompenhans, J. (1998). *Particle Image Velocimetry: A Practical Guide*. New York: Springer.

Videler, J. J. and Hess, F. (1984). Fast continuous swimming of two pelagic predators, saithe (*Pollachius virens*) and mackerel (*Scomber scombrus*): a kinematic analysis. *J. Exp. Biol.* **109**, 209–228.

Videler, J. J., Muller, U. K. and Stamhuis, E. J. (1999). Aquatic vertebrate locomotion: wakes from body waves. *J. Exp. Biol.* **202**, 3423–3430.

Walker, J. A. (1998). Estimating velocities and accelerations of animal locomotion: a simulation experiment comparing numerical differentiation algorithms. *J. Exp. Biol.* **201**, 981–995.

Walters, V. (1962). Body form and swimming performance in the scombroid fishes. *Am. Zool.* **2**, 143–149.

Webb, P. W. (1975). Hydrodynamics and energetics of fish propulsion. *Bull. Fish. Res. Bd Can.* **190**, 1–159.

Wilga, C. D. and Lauder, G. V. (1999). Locomotion in sturgeon: function of the pectoral fins. *J. Exp. Biol.* **202**, 2413–2432.

Wilga, C. D. and Lauder, G. V. (2000). Three-dimensional kinematics and wake structure of the pectoral fins during locomotion in leopard sharks *Triakis semifasciata*. *J. Exp. Biol.* **203**, 2261–2278.

Willert, C. E. and Gharib, M. (1991). Digital particle image velocimetry. *Exp. Fluids* **10**, 181–193.

Winter, D. A. (1989). *Biomechanics and Motor Control of Human Movement*. New York: John Wiley & Sons, Inc.

Wolfgang, M. J., Anderson, J. M., Grosenbaugh, M. A., Yue, D. K. P. and Triantafyllou, M. S. (1999). Near-body flow dynamics in swimming fish. *J. Exp. Biol.* **202**, 2303–2327.

Zar, J. H. (1984). *Biostatistical Analysis*. Englewood Cliffs, NJ: Prentice Hall.